The Concurrent Variability of East Asian Subtropical and Polar-front Jets and Its Implication for the Winter Climate Anomaly in China

Chuliang Xiao[1, 2], Yaocun Zhang[1], Brent M. Lofgren[3], and Yu Nie[4]

[1]School of Atmospheric Sciences, Nanjing University, Nanjing, China

[2]Cooperative Institute for Limnology and Ecosystems Research (CILER), University of Michigan, Ann Arbor, Michigan, USA

[3]NOAA Great Lakes Environmental Research Laboratory, Ann Arbor, Michigan, USA

[4]Beijing Climate Center, China Meteorological Administration, Beijing, China

Main point #1: The leading modes of zonal-mean zonal wind in East Asia and the concurrent existence of East Asian subtropical jet and polar-front jet.

Main point #2: Their concurrent variability can be interpreted as wave-mean flow interactions via synoptic-scale transient eddy activities.

Main point #3: A comprehensive understanding of the winter climate in China from the perspective of double jets.

Corresponding author address:

Yaocun Zhang, Ph.D.

yczhang@nju.edu.cn,

School of Atmospheric Sciences,

Nanjing University,

163 Xianlin Ave., Nanjing 210023, China

ABSTRACT

The variability of East Asian upper-level westerly jets in winter is studied with regard to the concurrent existence of subtropical jet (EASJ) and polar-front jet (EAPJ) using the National Centers for Environmental Prediction/National Center for Atmospheric Research reanalysis. In the distribution of jet occurrence revealed in 6-hourly data, two jet branches along 30°N and 55°N, corresponding to locations of EASJ and EAPJ respectively, are separated over the Tibetan Plateau. The leading two modes of zonal-mean zonal wind in East Asia extracted from a mass-weighted Empirical Orthogonal Function analysis are characterized by the intensity changes and location displacements of two jets. The key regions for EASJ and EAPJ are then defined to represent variabilities of these two jets. Correlation analysis indicates that the subseasonal variation of EAPJ precedes EASJ by around five days, which can be interpreted as wave-mean flow interactions via synoptic-scale transient eddy activities. Based on the pentad intensity indices of two jets, the concurrent variabilities of EASJ and EAPJ are investigated with typical temperature and precipitation anomalies in China. The results suggest that, by taking account of the two jets, we are able to get a more comprehensive understanding of the winter climate.

1. Introduction

The upper-level jet streams vary distinctively in East Asia which is characterized by the unique mechanical and thermodynamic conditions on Earth. In the cold season, two jets are located at the southern and northern flanks of the Tibetan Plateau (TP), namely, the East Asian subtropical jet (EASJ) and East Asian polar-front jet (EAPJ, also known as East Asian eddy-driven jet) respectively. The EASJ exhibits robust seasonal evolutions in location and intensity, which are accompanied by the transitions of the East Asian general atmospheric circulation pattern [*Yeh et al.,* 1958; *Li et al.,* 2004; *Zhang et al.,* 2006]. Comparatively, EAPJ is not as stable nor as strong as EASJ and experiences wide location variations in the polar-front zone, where it is characterized by synoptic-scale transient eddy activities [*Riehl,* 1962; *Lee and Kim,* 2003; *Zhang et al.,* 2008; *Ren et al.,* 2011].

In the climatological zonal-mean zonal wind, subtropical and polar-front jets are often differentiable in the Southern Hemisphere and Atlantic sector [*Bals-Elsholz et al.,* 2001], but not in the East Asia-Pacific sector where the subtropical jet is dominant [*Lee and Kim,* 2003; *Koch et al.,* 2006]. Most prior studies focused on EASJ, while the EAPJ has received relatively less attention. Regionally, as the most prominent feature in the upper troposphere, the EASJ relates to the seasonal transition of the atmospheric circulation and monsoon onset, as well as the launch of the rainy season over East Asia [*Yeh et al.,* 1958; *Yang et al.,* 2002; *Li et al.,* 2004]. Hemispherically, it acts as a waveguide between the North Atlantic and East Asia by trapping quasi-stationary Rossby waves originating from the North Atlantic Oscillation (NAO) [*Hoskins and Ambrizzi,* 1993; *Branstator,* 2002; *Watanabe,* 2004]. Substantial efforts have been devoted

to studying the variability of EASJ, in terms of meridional/zonal location displacement and intensity change, as well as its connection to the weather and climate in East Asia. *Li et al.* [2004] investigated the relationship between the onset of the East Asian summer monsoon and the northward jump of EASJ. *Lin and Lu* [2008] pointed out that a sudden jump of the EASJ from 40°N to north of 45°N happens in late July, corresponding to the end of the Japanese *Baiu*. Besides the meridional jump, the EASJ also exhibits significant zonal displacement. The diabatic heating from the TP is a major factor contributing to the zonal shift [*Kuang and Zhang*, 2005]. *Du et al.* [2008] demonstrated that the zonal position of the EASJ center is a useful indicator to the starting/ending time of the Chinese *Meiyu*. Together with the location movement, the intensity of EASJ varies with climate and climate change. *Kwon et al.* [2007] found that a decadal weakening of the EASJ interannual variability, since the 1990s, was connected with northward Rossby wave trains induced by the increased precipitation in Southern China. Meanwhile, barotropic energy conversion from basic flow to anomalous patterns may contribute to the weakening variability [*Lu et al.*, 2011].

Compared to the prevailing westerly in EASJ with the obvious jet axis and center, EAPJ is much weaker over the East Asian landmass and merges into EASJ over the North Pacific Ocean. Due to the transient feature, apparent changes in the jet intensity and location lead to an ambiguous mean position of EAPJ. In recent year, high-temporal resolution data has been used to identify polar-front jets from the perspective of jet core numbers [*Koch et al.*, 2006; *Zhang et al.*, 2008; *Schiemann et al.*, 2009; *Ren et al.*, 2010, 2011; *Pena-Ortiz et al.*, 2013]. More characteristics of EAPJ have been revealed and compared with those of its counterpart, EASJ.

The meridional wind component plays a crucial role in the formation and seasonal evolution of EAPJ [*Zhang et al.,* 2008], which is embedded in strong synoptic-scale transient eddy activities in East Asian midlatitude. The land surface in East Asia, dominated by arid and semi-arid deserts, leads to large fluctuations of low-level static stability and development of baroclinicity [*Ren et al.,* 2011].

Previous studies suggest that subtropical and polar-front jets are maintained by different dynamic mechanisms and they do not independently exist [*Lee and Kim,* 2003; *Li and Wettstein,* 2012; *Pena-Ortiz et al.,* 2013]. Due to the asymmetric distribution of westerlies in the Northern Hemisphere, the upper-level jets over East Asia possess distinctive features that significantly differ from the North Pacific and the North Atlantic. Studies from concurrent variations between EASJ and EAPJ reflects a more comprehensive conception of the East Asia monsoon system [*Liao and Zhang,* 2013; *Li and Zhang,* 2014; *Huang et al.,* 2014].

Since the subtropical jet is predominant over East Asia, studies on the upper-level jet and associated climatic effects were carried out based on a single subtropical jet, especially in the summer time [*Yeh et al.,* 1958; *Li et al.,* 2004; *Liao et al.,* 2004; *Kuang and Zhang et al.,* 2006; *Zhang et al.*, 2006]. *Yang et al.* [2002] and *Mao et al.* [2007] discussed the relation between the East Asian subtropical jet stream and winter climate anomalies. *Jhun and Lee* [2004] proposed a new East Asian winter monsoon index using the 300-hPa wind shear associated with the jet stream. Recently, a detailed comparison of the EASJ and EAPJ in winter season was conducted by *Ren et al.* [2011]. Studies with double jets suggested that the concurrent variability of EASJ and EAPJ can reflect a more comprehensive conception of the East Asia monsoon system, but

mainly focusing on the summer time [*Li and Zhang,* 2014; *Huang et al.,* 2014]. The winter precipitation in China exhibits distinct multiple-mode characteristics [e.g. *Yao et al.,* 2015], which cannot be adequately interpreted from a single jet. Based on those achievements mentioned above, we revisited the topic of upper-level jets and associated climate implications, attempting to gain insights on the concurrent existence of EASJ and EAPJ and to add new values to the understanding of the winter climate in the East Asian region.

The remainder of this paper is organized as follows. The reanalysis and observational data are introduced in section 2. Section 3 describes the methodologies of defining the EASJ and EAPJ. Their concurrent variation and associated climate impacts are discussed in Sections 4 and 5, respectively. Conclusions and discussion are presented in Section 5.

2. Data

The atmospheric circulation data were obtained from the National Centers for Environmental Prediction/National Center for Atmospheric Research (NCEP/NCAR) reanalysis data [*Kalnay et al.,* 1996] of winter (December-January-February) seasons from 1970 to 2010. The data have a horizontal resolution of 2.5° × 2.5° in longitude and latitude with 17 vertical levels. We use the 6-hourly and monthly-mean fields, as well as the data averaged for each pentad. The pentad data were created by consecutive 5-day averaging. Thus, every non-leap winter with 90 days is divided into 18 pentads. In a leap-year winter, the 18^{th} pentad is averaged for 6 days.

The daily temperature and precipitation at 738 stations from 1970 to 2000, provided by the National Meteorological Information Center of China, are also used to generate pentad time series in this study. Given that missing values exist in observations especially in winter precipitation, if no less than two observations are archived in a pentad period, then the pentad mean is averaged for the available days. A station will be selected if it has 18 pentad records in every winter. Finally, 645 (567) stations have full records of pentad temperature (precipitation) data.

3. Jet definitions

The upper-level jet is a narrow stream located from the upper troposphere to lower stratosphere, characterized by high wind speeds and large vertical and horizontal wind shears. In East Asia, the intensity of the time-mean wind gradually decreases from the westerly jet axis to the polar-front region. The EASJ is persistent and dominant in both the time-mean and high-frequency fields. Thus, in the time-mean wind field, the EAPJ can hardly be distinguished from the EASJ. Therefore, to explicitly describe the seasonal variation of the EAPJ, daily or higher-frequency data is needed. In previous studies, three methods have been used to define upper-level jets from the perspective of jet occurrence.

(a) Jet Occurrence Percentage (JOP) [*Koch et al.,* 2006]

If the wind speed in one grid is equal or larger than 30 m s^{-1} at one grid cell, a jet occurrence is defined at this cell. The jet occurrence number is counted at every grid cell. Then, the JOP is calculated as:

$$\mathrm{JOP} = \frac{Jet\ Occurrence\ Number}{Total\ Number\ of\ Time\ Intervals} \times 100\%$$

(b) Horizontal Jet Core Number (hJCN) [*Zhang et al.*, 2008; *Ren et al.*, 2010, 2011]

In the horizontal longitude-latitude plane, a jet core occurrence is defined if one specific grid cell satisfies the following conditions: (1) the wind speed at this grid cell is equal to or greater than 30 m s^{-1}; (2) the wind speeds at the surrounding eight grid cells are smaller than in this grid cell. These procedures are applied at every time to calculate the hJCN.

(c) Vertical Jet Core Number (vJCN) [*Schiemann et al.*, 2009; *Pena-Ortiz et al.*, 2013]

The vJCN is defined the same as the hJCN, but in the vertical pressure-latitude cross-section plane. In this method, vJCN is counted on every vertical level.

These three methods were used in the East Asian region to define the locations of EAPJ and EASJ. Figure 1 shows the climatological distributions of JOP, hJCN and vJCN, as well as the isotach. Here, JOP and hJCN are calculated at 300 hPa, and the vJCN is summed from 1000 hPa to 100 hPa. The time-mean wind field is dominated by strong wind speed on the south side of the TP, corresponding to the location of EASJ. The wind speed decreases gradually from EASJ axis to the north side of the TP where a weak isotach ridge extends westwards with velocity lower than 30 m s^{-1}. EAPJ can hardly be detected in the time-mean wind field. From jet occurrence, however, the locations of EAPJ and EASJ are well distinguished. In JOP field, a local maximum center representing the region of frequent jet occurrence (more than 30%) is located along the EAPJ axis, split from the belt of EASJ. The distribution of vJCN is similar to hJCN. Two belts of frequent jet cores are separated with a minimum zone over the TP. The method of vJCN

produces more jet cores than hJCN. From the distribution of zonal winds, EASJ seems to be a single consecutive westerly jet with an only center over the ocean. However, from the distribution of jet cores, EASJ exhibits striking wind fluctuations with multiple zonal hJCN centers along the southern flank of the TP. Although the wind speed over the land is much weaker than that over the ocean, the hJCN over the land are even stronger than that over the ocean, suggesting that there may be different dynamic mechanisms maintaining the land and ocean portions of EASJ [*Liao and Zhang,* 2013] (see more details in subsection 4.2).

4. Results

4.1. Modes of variability

The distributions of jet occurrence show that two jet belts are located on the south (30°N) and north (55°N) flanks of the TP. Studies on atmospheric low-frequency variability proposed useful indices and modes to describe the interaction between middle and high latitudes. *Rossby* [1939] introduced a simple "zonal index" to quantify the circulation intensity. *Wallace and Gutzler* [1981] documented the major anomaly patterns in the Northern Hemisphere winter in terms of teleconnection indices. As the most prominent variability in the extratropical atmosphere, annular modes are characterized by north-south shifts in atmospheric mass between the polar region and the middle latitude in both Hemispheres [*Thompson and Wallace,* 1998; 2000]. Compared with these hemispherical views, others conducted their studies with regional interests. *Jhun and Lee* [2004] defined an East Asian winter monsoon (EAWM) index using the meridional shear of zonal wind. *Eichelberger and Hartmann* [2007] investigated the zonal

asymmetries of the Northern Annular Mode, specifically concentrating on the differences between the zonal flow and the leading mode of variability over the Atlantic and Pacific sectors. Due to the unique mechanical and thermodynamic conditions, the annular mode-like variability in the East Asian region needs more specific attention.

Similarly to *Thompson and Wallace* [2000], we perform mass-weighted Empirical Orthogonal Function (EOF) analysis to determine the primary modes in the East Asian region. The mass-weighted zonal-mean zonal wind $[U]$ is calculated as

$$[U] = [u] \cdot \sqrt{\cos\varphi \cdot \Delta p}, \quad (1)$$

where $[u]$ is the zonal-mean zonal wind averaged from 60°E -160°E in winter, φ is latitude, and Δp is the vertical pressure interval. The leading two principal components (PCs) are extracted. Unlike *Thompson and Wallace* [2000], we regressed the weighted anomaly fields against the standardized PCs and obtain the orthogonal EOF modes. Figure 2 shows the leading two modes and corresponding PCs, which are well separated from the other modes based on the method of *North et al.* [1982].

(1) Spatial patterns. The EOF1 explaining 40.2% of the total variance depicts a meridional dipole structure around 300 hPa. The two centers coincide with the location of EASJ and EAPJ, respectively. EOF1 reveals that the intensities of EASJ and EAPJ vary inversely with each other. The EOF2 can explain 28.2% of the total variance and indicates the meridional displacement of EASJ and EAPJ, approaching or separating simultaneously.

(2) Time series. As the leading mode of the interannual variability in East Asia, the PC1 is highly related with EAWM index (correlation coefficient is -0.94) defined by *Jhun and*

Lee [2004] (see Table S1 for the correlations between PCs with other teleconnection indices). The PC2 is dominated by the multiannual variability.

Based on the PCs, we further analyze the zonal wind anomaly related to the leading modes (Figure S1). The zonal-mean zonal wind is regressed onto PC1 and PC2 to extract two independent variabilities. The first regression is characterized by a dipole mode, similar with the EOF1 pattern. The second regression pictures the multiannual variability of meridional displacements of EASJ and EAPJ. Besides the monthly wind, the associated transient feature of jet occurrence has been further examined. Figure 3 shows the difference of composite vJCN between strong and weak PC years. In presence of a strong (weak) subtropical jet, it is often the case that the EAPJ tends to separate from (merge with) the EASJ. Similarly, EOF2 could be reinterpreted as showing a meridional shift of the EASJ, with an impact on the EAPJ- either merged with the subtropical jet or clearly separated from it.

From the perspective of the thermal wind principle, the upper-level westerly jet is maintained by the meridional temperature gradient (MTG) below. The thermodynamic condition of the elevated TP regulates the upper-level jets. Figure 4 illustrates the composite anomaly of zonal-mean vertical cross section between strong and weak years based on the PC1 and PC2 time series. In the first mode, the middle atmosphere below the EASJ center cools down on the south side of the TP; the lower-to-middle layer warms up on the north side of the TP. The MTG under the EASJ is reduced and the MTG under EAPJ is enhanced, resulting in a weak EASJ and strong EAPJ. In the wind composite, when the zonal wind decreases in EASJ and increases in EAPJ, a north wind anomaly is induced in EASJ and a south wind anomaly in EAPJ. Compared to the

dipole heating in the first mode, the second mode is dominated by a strong cooling center over the TP which is associated with descending vertical flow.

For a better understanding of the second mode, the zonal wind on 300 hPa is regressed onto the PC2 to see the horizontal distribution of PC2-induced zonal wind anomaly (Figure 5a). The south side of EASJ axis and the north side of EAPJ axis are westerly anomalies, while the region between EASJ and EAPJ is covered by easterly anomalies, indicating the separation of EASJ and EAPJ. Meanwhile, the wind anomaly is related to a cooling TP and warming Siberia (Figure 5b).

4.2. Key regions for the EASJ and EAPJ

In section 3, EASJ and EAPJ are separated from the distribution of the jet occurrence using 6-hourly zonal winds. Then, the leading variability modes associated these two jets are revealed through the mass-weighted EOF analysis. Based on the jet occurrence and EOF patterns, the key regions of EASJ and EAPJ are defined to characterize their intensity changes. All three methods are in good agreement on the location of EAPJ around 55°N. However, obvious differences happen in EASJ. As the zonal wind moves eastward, the EASJ axis shifts northward. The JOP center coincides with the westerly center near southern Japan (Figure 1a), while the hJCN contains multiple centers lying on the EASJ axis (Figure 1b). Therefore, two sectors are chosen to describe the land (EASJ-L) and ocean (EASJ-O) portions of EASJ. The detailed information of key regions for EASJ and EAPJ are listed in Table 1. Then, the jet intensity is defined as the area-mean wind speed.

4.3. Correlation analysis

In contrast to the EASJ, dominated by westerlies, the EAPJ is comprised of almost equivalent zonal and meridional components [*Zhang et al.*, 2008]. As shown in Figure 4a, the intensified westerly in EAPJ is accompanied with strong southerly anomaly which tends to reduce the north wind component. The comparison of the zonal wind and the meridional wind in EAPJ is presented in Figure 6. The positive westerly is highly related with the negative northerly. In a common case, when the zonal wind increases in EAPJ, the meridional wind decreases at the same time. The magnitude of the interannual variation of the meridional wind component is close to the zonal wind component.

Because the zonal and meridional wind components are both important in EAPJ and are closely interrelated, their individual relation with the EASJ is further compared. Figure 7 shows the subseasonal variation of the correlation coefficients between the zonal (EAPJ_u), meridional (EAPJ_v) wind in EAPJ and the zonal wind in EASJ (EASJ_u). Both the EAPJ_u and EAPJ_v are anticorrelated with the EASJ in winter. Generally, the zonal wind in EAPJ has a stronger relation with EASJ than the meridional counterpart. In winter seasonal mean, these two correlations are significant. As a matter of convenience, only the zonal wind is used to quantify the intensity of EAPJ, as in EASJ.

In the interannual time scale, the EAPJ is highly related to the EASJ in winter, especially the ocean portion of EASJ. The correlation coefficient between the EAPJ intensity and the EASJ-L (EASJ-O) intensity is 0.54 (0.83). In order to examine the subseasonal relationship between EAPJ and EASJ, we extend the winter season to seven months from October to April and obtain

42-pentad time series of EAPJ and EASJ. The annual variation of lead-lag correlation between EAPJ and EASJ is shown in Figure 8. Generally, the EAPJ is anticorrelated with the EASJ with lead periods ranging from 0 to 20 days. In most years, the EAPJ leads the EASJ-O by five days, which indicate synoptic-scale waves propagating along the East Asian trough from the north side of the TP to the oceanic region. When the EAPJ experiences an enhancement, the EASJ over the ocean tends to be reduced five days later. This lead correlation between EAPJ and EASJ-O is interrupted after the mid-1990s, which is in agreement with the weakening interannual variability of the first mode. The EAPJ leads the EASJ-L by about 0-20 days. This leading relationship becomes more significant after the 1990s. Since the EASJ center is located over the ocean and EAPJ possesses a stronger relationship with the EASJ-O, the oceanic portion of the EASJ is selected to represent EASJ in the following analysis. To get a more robust result on the subseasonal variability, we repeated the same correlation analysis (Figure S3) based on the Japanese 55-year Reanalysis (JRA-55) [*Kobayashi et al.*, 2015]. The above result from NCEP/NCAR was further verified by JRA-55.

4.4. Synoptic-scale transient eddy activities

As an eddy-driven jet, the EAPJ is associated with strong synoptic-scale transient eddy activities in the cold seasons [*Ren et al.,* 2010, 2011; *Xiao and Zhang,* 2012, 2015]. The correlation analysis indicates that the EAPJ change leads the EASJ by five days. In this subsection, we try to understand the concurrent variation of EAPJ and EASJ from the perspective of wave-mean flow interaction.

The transient eddy kinetic energy (EKE) is calculated to represent synoptic-scale transient eddy activities in the following equation,

$$EKE = \overline{u'^2 + v'^2}\ , (2)$$

where u and v are the zonal and meridional wind component, the prime denotes 2-8 day bandpass filtering, and the overbar means temporal average in winter. A useful diagnostic tool is utilized to analyze the transient eddy and its feedback onto mean flow. Here we will provide a simple interpretation of the eddies' impact on the westerlies and the interaction between EAPJ and EASJ. Introduced by Hoskins et al. (1983), the eddy vorticity flux convergence can be written in terms of $\boldsymbol{E} = \left(\overline{v'^2 - u'^2}, -\overline{v'u'}\right)$, which can be considered as an effective westerly momentum flux. There is a forcing on the mean horizontal circulation to increase (decrease) westerly mean flow where the vector $\boldsymbol{E}$ is divergent (convergent).

The climatological distributions of transient EKE, vector $\boldsymbol{E}$, and its divergence are presented in Figure 9. A vigorous EKE branch is accompanied by strong westerly momentum flux, vector $\boldsymbol{E}$, expanding southeastward from the polar-front zone to the subtropical jet center. The EKE on the south side of the TP becomes much weaker, where the EAPJ is maintained by the thermal contrast and fewer synoptic-scale eddies occur. The vector $\boldsymbol{E}$ represents the direction of wave propagation; the resulting zonal momentum transfer is in the direction opposite to Rossby wave-like disturbances. The eddy momentum from the EASJ center over the ocean is transferred to the EAPJ region. The vector $\boldsymbol{E}$ is divergent in the polar-front zone, corresponding to a forcing on the mean flow to increase the intensity of EAPJ.

4.5. The indices of the EASJ and EAPJ

Through the preceding investigation, we define two jet streams in the East Asian region, EASJ and EAPJ (Figure S2). Their magnitude and location change concurrently, as revealed in the leading variability modes. Correlation analysis indicates that the zonal wind in EAPJ is strongly related to the EASJ over the ocean. Based on the area-mean zonal wind in two selected key regions, two pentad time series are calculated to represent the intensity indices of EAPJ and EASJ for 30 winters. The magnitude of the mean state of EAPJ is much weaker than the EASJ. The magnitude of interannual variation, due to the transient features of the EAPJ, is even stronger than the EASJ.

5. *Climatic impacts on temperature and precipitation in China*

The jet-related weather/climate impact is one of the most interesting topics attracting extensive attention. Most prior studies are conducted with a single jet, such as the subtropical jet in East Asia. Recently, results with regard to two jets indicate that the concurrent variation of EAPJ and EASJ plays an important role in the precipitation anomaly in winter and in Meiyu season [*Liao and Zhang*, 2013; *Li and Zhang*, 2014].

With the intensity indices in section 4e, the climatic effects from the perspective of the concurrent variation of EAPJ and EASJ are investigated in terms of temperature and precipitation in China. Based on two standardized indices, four configurations are defined: strong EAPJ/ strong EASJ (SS), weak EAPJ/ weak EASJ (WW), weak EAPJ/strong EASJ (WS), and

strong EAPJ/weak EASJ (SW) (Table 2). Taking account of both the sample number and diversity, we choose the critical value 0.8 as the threshold to select the anomaly pentads into four configurations. As it is mentioned above that the EAPJ is anticorrelated with the EASJ, the out-of-phase configurations (WS and SW) contain more pentads. According to the four configurations listed in Table 2, the corresponding temperature and precipitation anomalies are composited to show the connection between the upper-level jets and the typical surface climate patterns in China.

Figure 10 shows the composite surface temperature anomalies in the four different configurations. When the EAPJ becomes weak (Figs. 10b, c), the numerical values of EAPJ_u and EAPJ_v decrease while the absolute value of the meridional wind component in EAPJ increases, meaning enhanced cold air from the polar region. So, in these two cases, the surface is dominated by cool anomalies. The difference between Figure 10b and Figure 10c is that when the EASJ is strong the cooling can reach as far as the South China coast with a larger magnitude. When the EAPJ is strong and the EASJ is weak (Figure 10d), most of China will experience a significant warming period, especially in the Northeast.

Compared with the nation-wide temperature anomaly, the precipitation anomaly associated with the concurrent variation of EAPJ and EASJ is concentrated in South and East China (Figure 11), because the winter precipitation in North and Northwest China (mostly in the form of snowfall) is much weaker than that in South and East China. In simple terms, the precipitation results from the combination of vapor and condensation conditions. The northerly component of the EAPJ brings cold air masses (also known as “cold surge”) from the polar region [*Yao et al.*,

2015]. The EASJ can provide warm moisture from Bengal Bay which interacts with the southward air mass, causing different precipitation anomalies in China. When the EAPJ and EASJ are strong (Figure 11a), Southern and Eastern China will become dry, and vice versa (Figure 11b). Sometimes, when the EAPJ is strong (Figs. 11 a, d), regardless if the EASJ, South China will have less precipitation. Generally, a strong EASJ is not favorable for the precipitation. Even though in some cases the EAPJ brings cold air, a strong EASJ will reduce the precipitation in the Yangtze River Basin (Figure 11c). The corresponding temperature and precipitation anomalies in China based on four different configurations of EASJ and EAPJ are summarized in Table 3.

In order to examine the connection between the concurrent variability of the upper-level jets and the large-scale thermodynamics in boreal winter, the atmospheric circulation anomalies associated those four configurations are illustrated in Figure 12. When EAPJ and EASJ are both strong (weak), the Northwestern Pacific is dominated by a cyclonic (anticyclonic) anomaly at 500 hPa, increasing (decreasing) the zonal wind on the south side while decreasing (increasing) the zonal wind on the north side; the Southern China is covered by a divergent (convergent) anomaly in the low-level atmosphere, resulting a dry (wet) winter as in Figure 11 (a) (in Figure 11 (b)). In a more common scenario when EAPJ is weak (strong) and EASJ is strong (weak), a cyclonic (anticyclonic) anomaly at 500 hPa extents eastwards from East Asia to Central Pacific, which is accompanied with an anticyclonic (cyclonic) anomaly in the Siberia, causing cold and wet (warm and dry) winter in Southern China.

6. Conclusions and discussion

In this study, the EAPJ and EASJ are investigated with regard to their concurrent variation in winter by using NCEP/NCAR reanalysis data. The EAPJ and EASJ are detected in statistical methods of jet occurrence from 6-hourly data. Then, the dynamical mechanism of their interaction is interpreted from the perspective of synoptic-scale transient eddy activity. Based on the intensity indices of the two jets, the associated climate impacts on subseasonal temperature and precipitation in China are compared in different configurations of EAPJ and EASJ. The major results can be synthesized as follows:

(1) Through the calculation of jet occurrence, two jet branches at 300 hPa, corresponding to the EAPJ and EASJ, are separated over the TP. The jet occurrence frequency is more than 30% in EAPJ even though no wind speed center is seen in the climatological wind field. Multiple hJCN centers lie on the EASJ axis. The hJCN centers in the land portion of EASJ are stronger than that in the EASJ center, indicating the dynamic difference between the land and ocean portions of EASJ.

(2) The leading modes of the zonal-mean zonal wind in East Asia are studied by mass-weighted EOF analysis, which are characterized by a magnitude change and location displacement of EAPJ and EASJ. The first mode represents the variability of the East Asia winter monsoon.

(3) According to the distribution of jet occurrence, the key regions for EAPJ and EASJ are defined to quantify their intensities. In contrast with EASJ, dominated by westerlies, EAPJ consists of westerly and northerly components, related to each other. Correlation analysis

indicates that subseasonal variation of EAPJ leads EASJ by around five days. The concurrent variation of EAPJ and EASJ can be interpreted from the perspective of wave-mean flow interaction via synoptic-scale transient eddy activities.

(4) Based on the intensity indices of the two jets, four concurrent configurations of EAPJ and EASJ are selected from the pentad time series. In each configuration, the corresponding temperature and precipitation anomalies are compared by using the gauged observations. The results suggest that by considering both jets, we can get a more comprehensive understanding of the winter climate in China.

As an important part of the East Asia monsoon circulation system, the upper-level jet is also affected by internal and external factors. The heating anomaly from snowpack and precipitation, as well as remote teleconnections from atmospheric and oceanic oscillations, can exert strong impacts on the jet location and intensity, which also affects the concurrent variation of EAPJ and EASJ at the same time. With the weakening of East Asian winter monsoon, the interannual variability of the first mode of the zonal-mean zonal wind in East Asia undergoes a striking reduction since the mid-1990s, giving rise to the decadal variability, which needs further efforts to explain. The future responses of the upper-level jets and their concurrent variability to global warming will be examined in following work.

Acknowledgments. We thank the National Centers for Environmental Prediction/National Center for Atmospheric Research for providing reanalysis data. This work was jointly supported by the National Natural Science Foundation of China (grants 41475092 and 41130963) and the Jiangsu Collaborative Innovation Center for Climate Change. Figures were created with the NCAR Command Language (Version 6.1.2) [Software], (2013) Boulder, Colorado: UCAR/NCAR/CISL/VETS. http://dx.doi.org/10.5065/D6WD3XH5. All data and codes in this paper are available upon request to Dr. Chuliang Xiao (cxiao@umich.edu). The comments of the Editor and three anonymous reviewers led to improvements in the quality of this manuscript.

References

Bals-Elsholz, T. M., E. H. Atallah, L. F. Bosart, T. A. Wasula, M. J. Cempa, and A. R. Lupo (2001), The wintertime Southern Hemisphere split jet: Structure, variability, and evolution, *J. Climate*, *14*, 4191–4215.

Branstator, G. (2002), Circumglobal teleconnections, the jet stream waveguide, and the North Atlantic Oscillation, *J. Climate*, *15*, 1983–1910.

Du, Y., Y. Zhang, and Z. Xie (2009), Impacts of the zonal position of the East Asian westerly jet core on precipitation distribution during Meiyu of China, *Acta Meteo. Sinica*, *23*, 506-516.

Eichelberger, S. J., and D. L. Hartmann, 2007: Zonal jet structure and the leading mode of variability, *J. Climate*, *20*, 5149–5163, doi:10.1175/JCLI4279.1.

Hoskins, B. J., and T. Ambrizzi (1993), Rossby wave propagation on a realistic longitudinally varying flow, *J. Atmos. Sci.*, *50*, 1661-1671.

Hoskins, B. J., I. N. James, and G. H. White (1983), The shape, propagation and mean-flow interaction of large-scale weather systems. *J. Atmos. Sci.*, *40*, 1595–1612.

Huang, D., J. Zhu, Y. Zhang, and A. Huang (2014), The different configurations of the East Asian polar front jet and subtropical jet and the associated rainfall anomalies over Eastern China in summer, *J. Climate*, *27*, 8205–8220.

Jhun, J.-G., and E.-J. Lee (2004), A new East Asian winter monsoon index and associated characteristics of the winter monsoon, *J. Climate*, *17*, 711–726.

Kalnay, E., et al. (1996), The NCEP/NCAR 40-Year Reanalysis Project, *Bull. Amer. Meteor. Soc.*, *77*, 437–471.

Kobayashi, S., Y. Ota, Y. Harada, A. Ebita, M. Moriya, H. Onoda, K. Onogi, H. Kamahori, C. Kobayashi, H. Endo, K. Miyaoka, and K. Takahashi (2015), The JRA-55 Reanalysis: General specifications and basic characteristics, *J. Meteor. Soc. Japan*, *93*, 5-48, doi:10.2151/jmsj.2015-001.

Koch, P., H. Wernli, and H. C. Daves (2006), An event-based jetstream climatology and typology, *Int. J. Climatol.*, *26*, 283–301.

Kwon, M., J.-G. Jhun, and K.-J. Ha (2007), Decadal change in East Asian summer monsoon circulation in the mid-1990s, *Geophys. Res. Lett.*, *34*, L21706, doi:10.1029/2007GL031977.

Kuang, X., and Y. Zhang (2005), Seasonal variation of the East Asian subtropical westerly jet and its association with the heating field over East Asia, *Adv. Atmos. Sci.*, *22*, 831–840.

Kuang, X., and Y. Zhang (2006), Impact of the position abnormalities of East Asian subtropical westerly jet on summer precipitation in middle-lower reaches of Yangtze River, *Plateau Meteorology*, 25, 382-389. (in Chinese)

Lee, S., and H.-K. Kim (2003), The dynamical relationship between subtropical and eddy-driven jets, *J. Atmos. Sci.*, *60*, 1490-1530.

Li, C., J.-T. Wang, S.-Z. Lin, and H. -R. Cho (2004), The relationship between East Asian summer monsoon activity and northward jump of the upper westerly jet location, *Chinese J. Atmos. Sci.*, *28*, 641-658.

Li, C., and J. J. Wettstein (2012), Thermally driven and eddy-driven jet variability in reanalysis, *J. Climate*, *25*, 1587–1596.

Li, L., and Y. Zhang (2014), Effects of different configurations of the East Asian subtropical and polar front jets on precipitation during Meiyu season, *J. Climate*, *27*, 6660–6672, doi:10.1175/JCLI-D-14-00021.1.

Liao, Z., and Y. Zhang (2013), Concurrent variation between the East Asian subtropical jet and polar front jet during persistent snowstorm period in 2008 winter over southern China, *J. Geophys. Res. Atmos.*, *118*, 6360–6373, doi:10.1002/jgrd.50558.

Lin, Z., and R. Lu (2008), Abrupt northward jump of the East Asian upper-tropospheric jet stream in mid-summer, *J. Meteor. Soc. Japan*, *86*, 857–866.

Lu, R., H. Ye, and J.-G. Jhun (2011), Weakening of interannual variability in the summer East Asian upper-tropospheric westerly jet since the mid-1990s, *Adv. Atmos. Sci.*, *28*, 1246–1258. doi: 10.1007/s00376-011-0222-5.

Mao, R., D. Gong, and Q. Fang (2007), Influences of the East Asian jet stream on winter climate in China, *Journal of Applied Meteorological Science*, 18, 137-146. (in Chinese)

North, G. R., T. L. Bell, R. F. Cahalan, and F. J. Moeng (1982), Sampling errors in the estimation of empirical orthogonal functions, *Mon. Wea. Rev.*, *110*, 699–706.

Pena-Ortiz, C., D. Gallego, P. Ribera, P. Ordonez, and M. D. C. Alvarez-Castro (2013), Observed trends in the global jet stream characteristics during the second half of the 20th century, *J. Geophys. Res.*, *118*, 2702-2713, doi:10.1002/jgrd.50305.

Ren, X., X. Yang, and C. Chu (2010), Seasonal variations of the synoptic-scale transient eddy activity and polar front jet over East Asia, *J. Climate, 23*, 3222–3233.

Ren, X., X. Yang, T. Zhou, and J. Fang (2011), Diagnostic comparison of winter time East Asian subtropical jet and polar-front jet: Large-scale characteristics and transient eddy activities, *Acta Meteor. Sinica.*, *25*, 21–33.

Riehl, H. (1962), *Jet Streams of the Atmosphere*. Tech. Rep. 32, Department of Atmospheric Science, Colorado State University, 177pp.

Rossby, C. G. (1939), Relation between variations in the intensity of the zonal circulation of the atmosphere and the displacements of the semi-permanent centers of action, *J. Mar. Res.*, *2*, 38–55.

Schiemann, R., D. Lüthi, and C. Schär (2009), Seasonality and interannual variability of the westerly jet in the Tibetan Plateau region, *J. Climate*, *22*, 2940–2957.

Thompson, D. W. J., and J. M. Wallace (1998), The Arctic Oscillation signature in the wintertime geopotential height and temperature fields, *Geophys. Res. Lett.*, *25*, 1297–1300, doi: 10.1029/98GL00950.

Thompson, D. W. J., and J. M. Wallace (2000), Annular modes in the extratropical circulation. Part I: Month-to-month variability, *J. Climate*, *13*, 1000–1016.

Wallace, J. M., and D. S. Gutzler (1981), Teleconnections in the geopotential height field during the Northern Hemisphere winter, *Mon. Wea. Rev*, *109*, 784–812.

Watanabe, M. (2004), Asian Jet Waveguide and a downstream extension of North Atlantic Oscillation, *J. Climate*, *17*, 4674–4691.

Xiao, C., and Y. Zhang (2012), The East Asian upper-tropospheric jet streams and associated transient eddy activities simulated by a climate system model BCC-CSM1.1, *Acta Meteor. Sinica*, *26*, 700-716, doi:10.1007/s13351-012-0603-4.

Xiao, C., and Y. Zhang (2015), Projected changes of wintertime synoptic-scale transient eddy activities in the East Asian eddy-driven jet from CMIP5 experiments, *Geophys. Res. Lett.*, *42*, doi:10.1002/2015GL064641.

Yang, S., K.-M. Lau, and K.-M. Kim (2002), Variations of the East Asian jet stream and Asian-Pacific-American winter climate anomalies, *J. Climate*, *15*, 306–325.

Yao, Y., H. Lin, and Q. Wu (2015), Subseasonal variability of precipitation in China during boreal winter, *J. Climate*, *28*, 6548–6559.

Yeh, D., S. Tao, and M. Li (1958), The abrupt change of circulation over Northern Hemisphere during June and October, *Acta Meteor. Sinica*, *29*, 250-263.

Zhang, Y., X. Kuang, W. Guo, and T. Zhou (2006), Seasonal evolution of the upper-tropospheric westerly jet core over East Asia, *Geophys. Res. Lett.*, *33*, L11708, doi:10.1029/2006GL026377.

Zhang, Y., D. Wang, and X. Ren (2008), Seasonal variation of the meridional wind in the temperate jet stream and its relationship to the Asian Monsoon, *Acta Meteorologica Sinica*, *24*, 446-454.

Table and Figure Captions:

Table 1. The key regions for the EAPJ and EASJ. EASJ-L and EASJ-O are the land and ocean portions of EASJ, respectively.

Table 2. The numbers of the anomaly pentad in which absolute values of the standardized EASJ and EAPJ intensity index surpass specified thresholds for four different configurations of EASJ and EAPJ. The first (second) alphabet represents the strong or weak EASJ (EAPJ) index. (For example, SS means the pentad with strong EASJ and strong EAPJ intensity index. The value 0.8 is chosen as the threshold for the composite analysis.)

Table 3. The corresponding temperature and precipitation anomalies in China to four different configurations of EASJ and EAPJ.

Figure 1. Climatological distributions of (a) jet *occurrence* percentage, (b) horizontal jet core number at 300 hPa and (c) vertical jet core number (see the text for detailed definition). The contours are the horizontal velocity (m s^{-1}) at 300 hPa. The 3000-m orographic outline of the Tibetan Plateau is denoted by the thick solid contour. The meridional wind maxima are presented in two thick lines, corresponding to the axis of EAPJ and EASJ, respectively.

Figure 2. (a) The first EOF mode (EOF1, m s^{-1}) and corresponding principle component (PC1) of zonal wind averaged from 60°E to 160°E in winter. (b) same as (a), but for the second mode. The contour indicates the zonal-mean zonal wind with interval of 5 m s^{-1}.The vertical solid line is the westerly axis in meridional direction. The two circles with cross at 300 hPa donate the subtropical and temperate jet cores, respectively. The zonal mean orography is dark shaded. The 5-year running mean of the PC time series is presented in the thick line.

Figure 3. (a) The difference (shading) of composite vJCN between strong and weak years based on PC1 time series. (b) Same as (a), but for PC2 time series. The contours denote the horizontal velocity (m s^{-1}) at 300 hPa.

Figure 4. (a) The zonal-mean vertical cross section difference between strong and weak years based on PC1. Vertical wind is presented in vector (m s^{-1}, the vertical component multiply by a factor of 100) and temperature in shading (°C). (b) same as (a), but based on PC2.

Figure 5. (a) The zonal wind on 300 hPa regressed on PC2 (m s^{-1}). (b) The correlation coefficient between land surface temperature and PC2. The light (deep) shading areas indicate statistical significant at 95% (99%) confidence level.

Figure 6. The annual variation of the area-mean (70-110°E, 40-60°N) zonal wind (black line, m s^{-1}) and meridional wind (red line, m s^{-1}) components at 300 hPa in EAPJ in winter.

Figure 7. The subseasonal variation of the correlation coefficient between the zonal wind in EASJ (EASJ_u) and the zonal wind in EAPJ (EAPJ_u, solid line), and the meridional wind in EAPJ (EAPJ_v, dash line). The horizontal line denotes the level of 95% confidence.

Figure 8. (a) The annual variation of the lead-lag correlation between the area-mean zonal wind in EAPJ and EASJ-O. The Y coordinate is the days when EAPJ lags EASJ-O. (b) same as (a), but for the relation between the area-mean zonal wind in EAPJ and EASJ-L.

Figure 9. Climatological distributions of transient EKE (shading, m^2 s^{-2}), vector $\boldsymbol{E}$ (m^2 s^{-2}), and the divergence of $\boldsymbol{E}$ (contour, 10^{-5} m s^{-2}) at 300 hPa.

Figure 10. Composite surface temperature anomalies (°C) in China for different matchups of EASJ and EAPJ (listed in Table 2). The open circle denotes the station statistical significant at 95% confidence level with Student's *t*-test.

Figure 11. Same as Figure 10, but for the precipitation anomalies (mm).

Figure 12. (a) Composite circulation anomalies for SS (SS pentads mean minus the climatology). The geopotential height (gpm) at 500 hPa is denoted by contours, air temperature (°C) at 850 hPa by shaded areas, and wind at 850 hPa by vectors (m s^{-1}). (b) , (c), and (d) for WW, WS, and SW, respectively.

Table 1. The key regions for the EAPJ and EASJ. EASJ-L and EASJ-O are the land and ocean portions of EASJ, respectively.

Jet Name	Region
EAPJ	70º-110ºE, 50º-60ºN
EASJ-L	70º-110ºE, 25º-30ºN
EASJ-O	120º-160ºE, 25-35ºN

Table 2. The numbers of the anomaly pentad in which absolute values of the standardized EASJ and EAPJ intensity index surpass specified thresholds for four different configurations of EASJ and EAPJ. The first (second) alphabet represents the strong or weak EASJ (EAPJ) index. (For example, SS means the pentad with strong EASJ and strong EAPJ intensity index. The value 0.8 is chosen as the threshold for the composite analysis.)

Threshold	SS	WW	WS	SW
0.5	36	32	88	62
0.8	**13**	**16**	**45**	**32**
0.9	6	11	35	22

Table 3. The corresponding temperature and precipitation anomalies in China to four different configurations of EASJ and EAPJ.

EAPJ	EASJ	Temperature	Precipitation
Strong	Strong	Cooling(Northeastern, South Xinjiang)	Dry(South Yangtze River)
Weak	Weak	Cooling(Mid-southern, North Xinjiang)	Wet(South Yangtze River)
Weak	Strong	Cooling(Inner Mongolia, Southern)	Dry(Yangtze River), Wet(Southern)
Strong	Weak	Warming(Nationwide)	Dry(Southern)

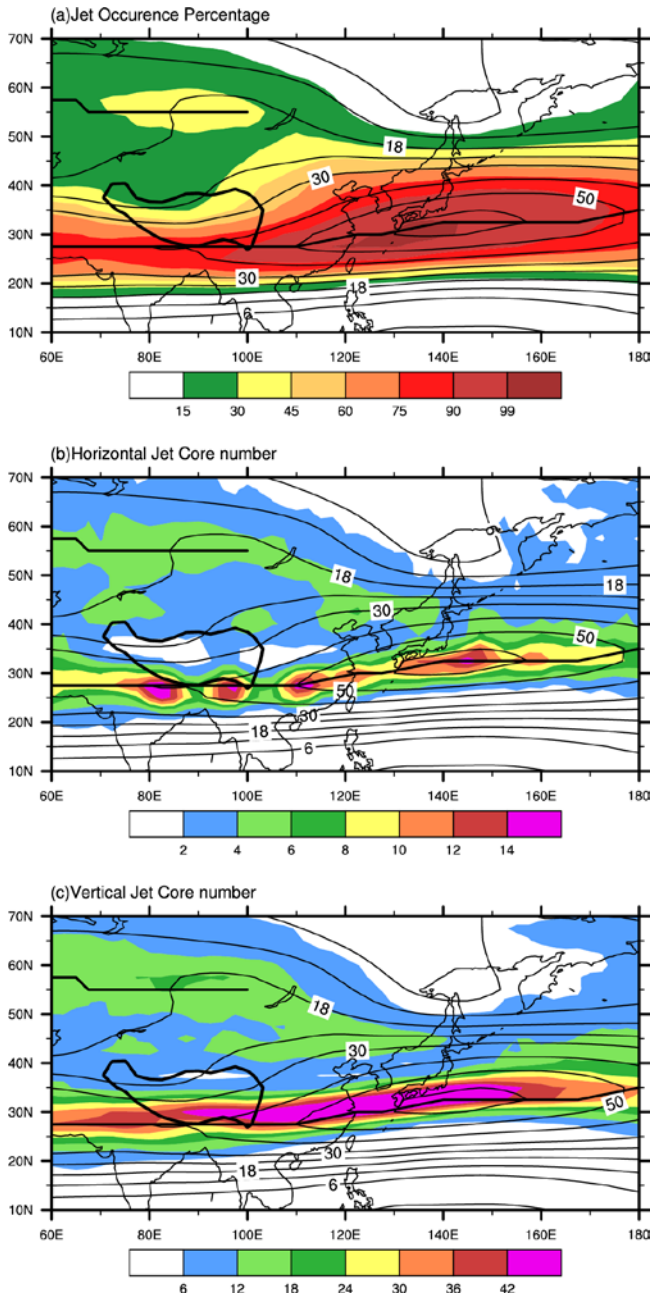

Figure 1. Climatological distributions of (a) jet *occurrence* percentage, (b) horizontal jet core number at 300 hPa and (c) vertical jet core number (see the text for detailed definition). The contours are the horizontal velocity (m s^{-1}) at 300 hPa. The 3000-m orographic outline of the

Tibetan Plateau is denoted by the thick solid contour. The wind maxima in the meridional direction are presented in two thick lines, corresponding to the axis of EAPJ and EASJ, respectively.

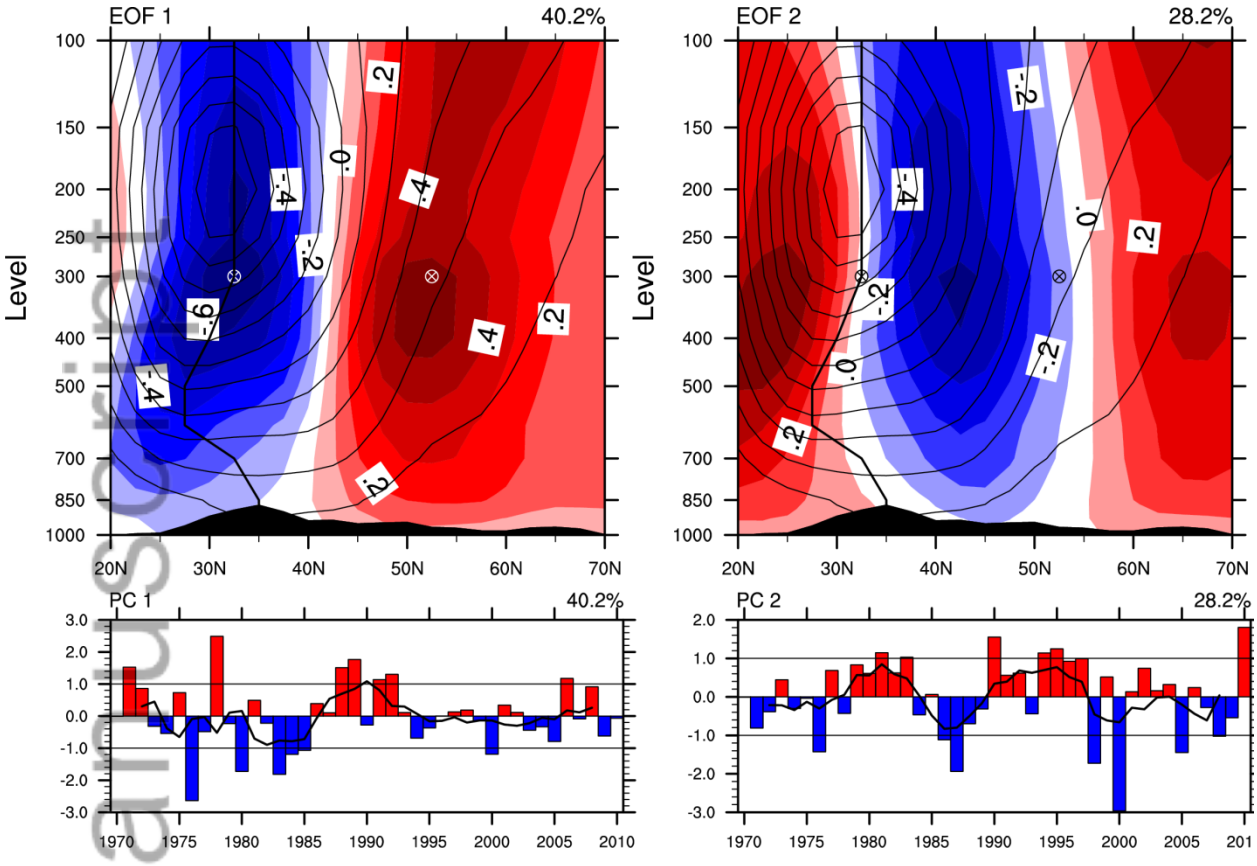

Figure 2. (a) The first EOF mode (EOF1, m s^{-1}) and corresponding principle component (PC1) of zonal wind averaged from 60°E to 160°E in winter. (b) same as (a), but for the second mode. The contour indicates the zonal-mean zonal wind with interval of 5 m s^{-1}.The vertical solid line is the westerly axis in meridional direction. The two circles with cross at 300 hPa donate the subtropical and temperate jet cores, respectively. The zonal mean orography is dark shaded. The 5-year running mean of the PC time series is presented in the thick line.

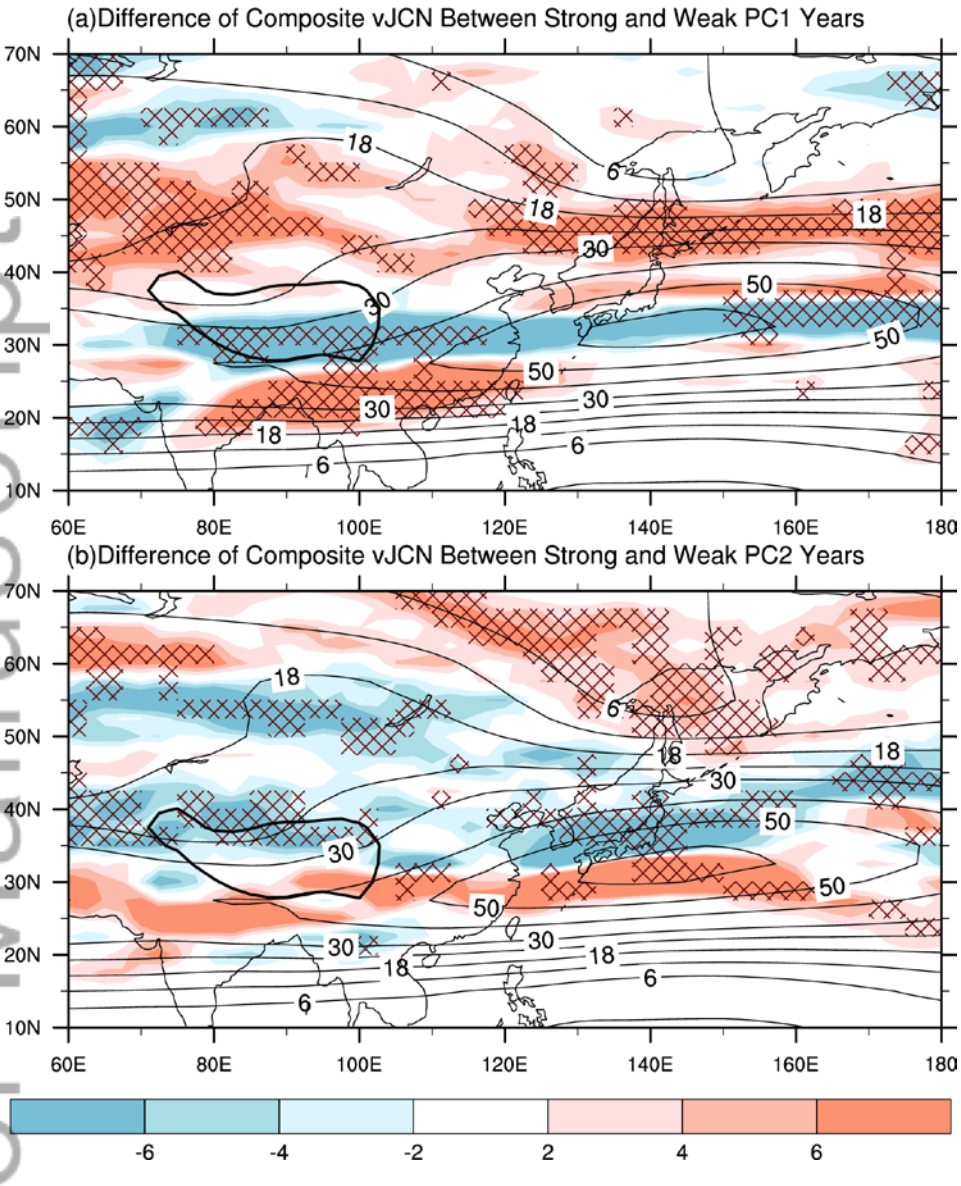

Figure 3. (a) The difference (shading) of composite vJCN between strong and weak years based on PC1 time series. (b) Same as (a), but for PC2 time series. The contours denote the horizontal velocity (m s^{-1}) at 300 hPa. The cross denotes the grid statistical significant at 95% confidence level with Student's *t*-test.

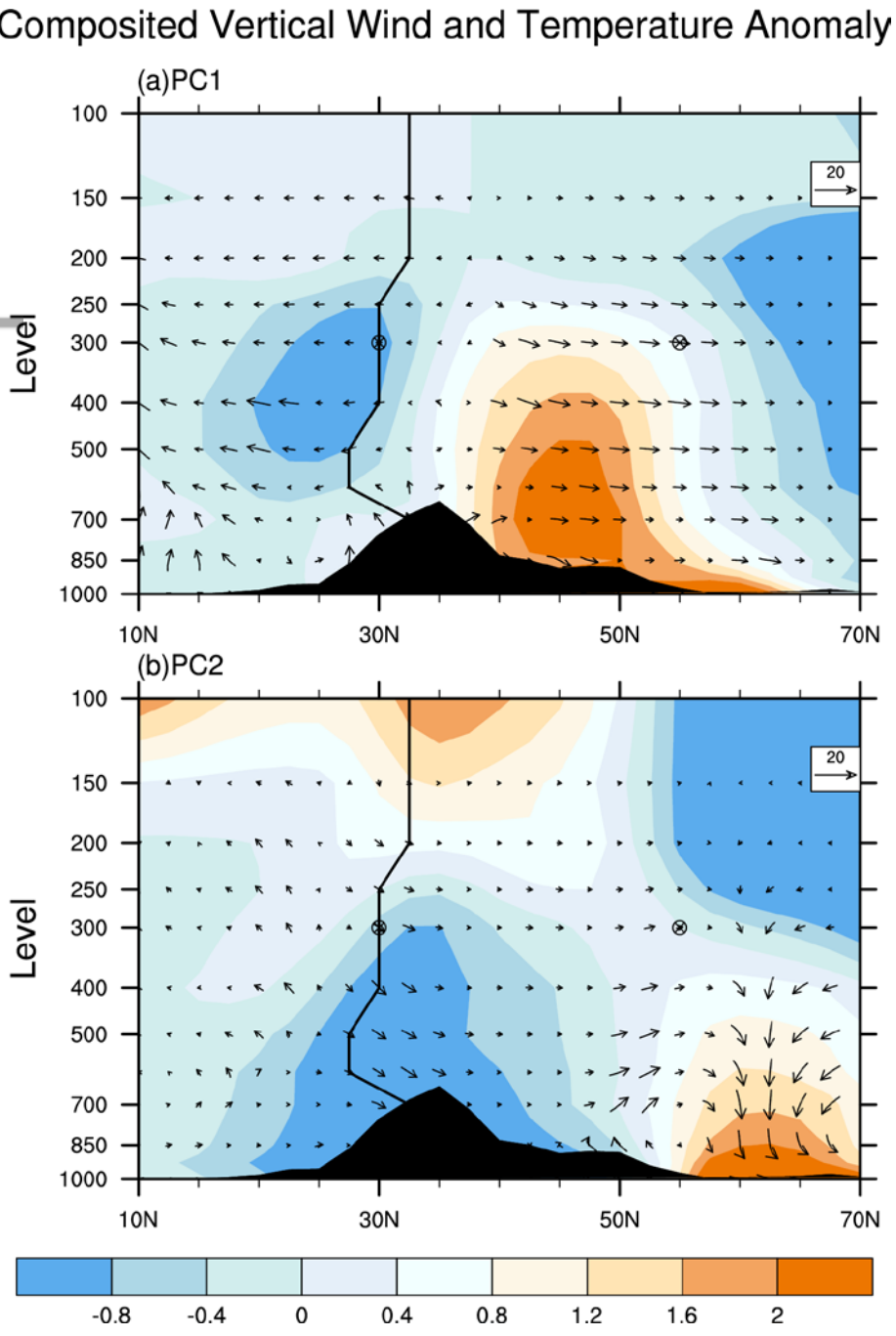

Figure 4. (a) The zonal-mean vertical cross section difference between strong and weak years based on PC1. Vertical wind is presented in vector (m s^{-1}, the vertical component multiply by a factor of 100) and temperature in shading (°C). (b) same as (a), but based on PC2.

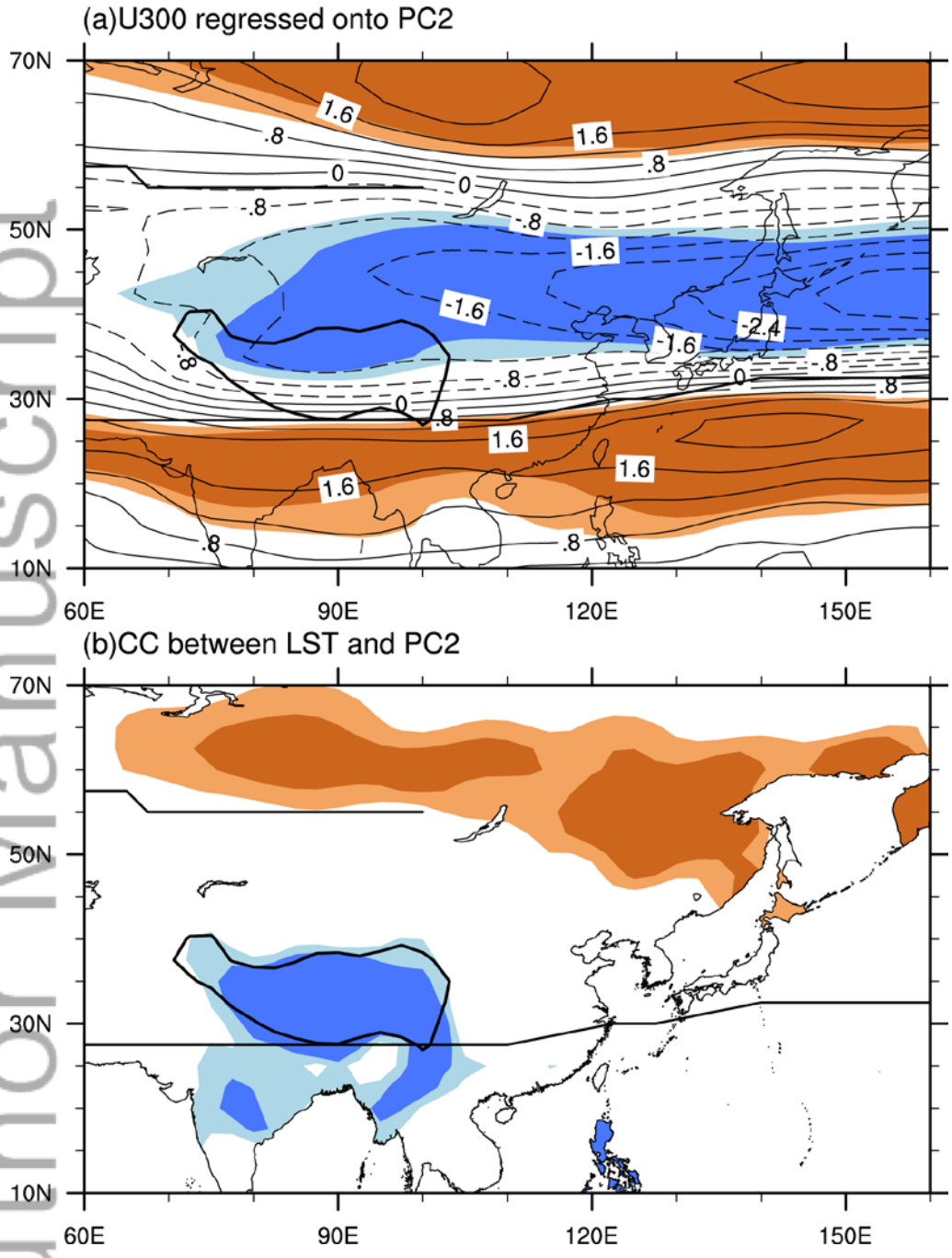

Figure 5. (a) The zonal wind on 300 hPa regressed on PC2 (m s^{-1}). (b) The correlation coefficient between land surface temperature and PC2. The light (deep) shading areas indicate statistically significant at 95% (99%) confidence level based on Student's *t*-test.

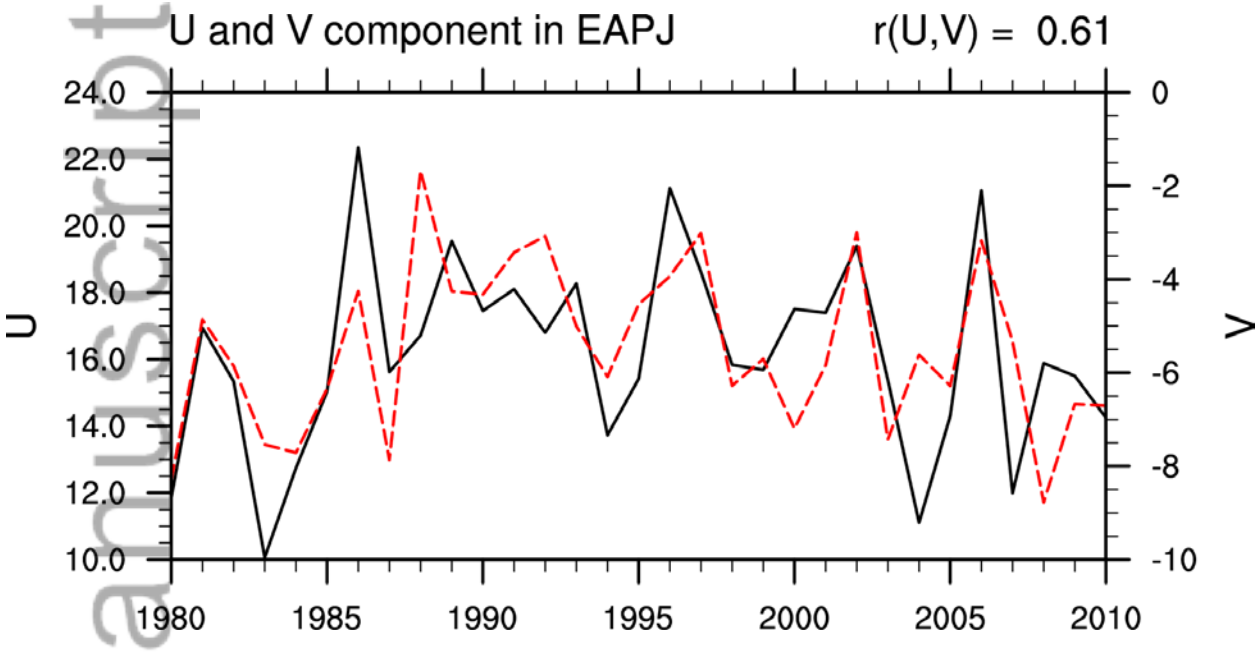

Figure 6. The interannual variation of the area-mean (70-110°E, 40-60°N) zonal wind (black line, m s^{-1}) and meridional wind (red line, m s^{-1}) components at 300 hPa in EAPJ in winter.

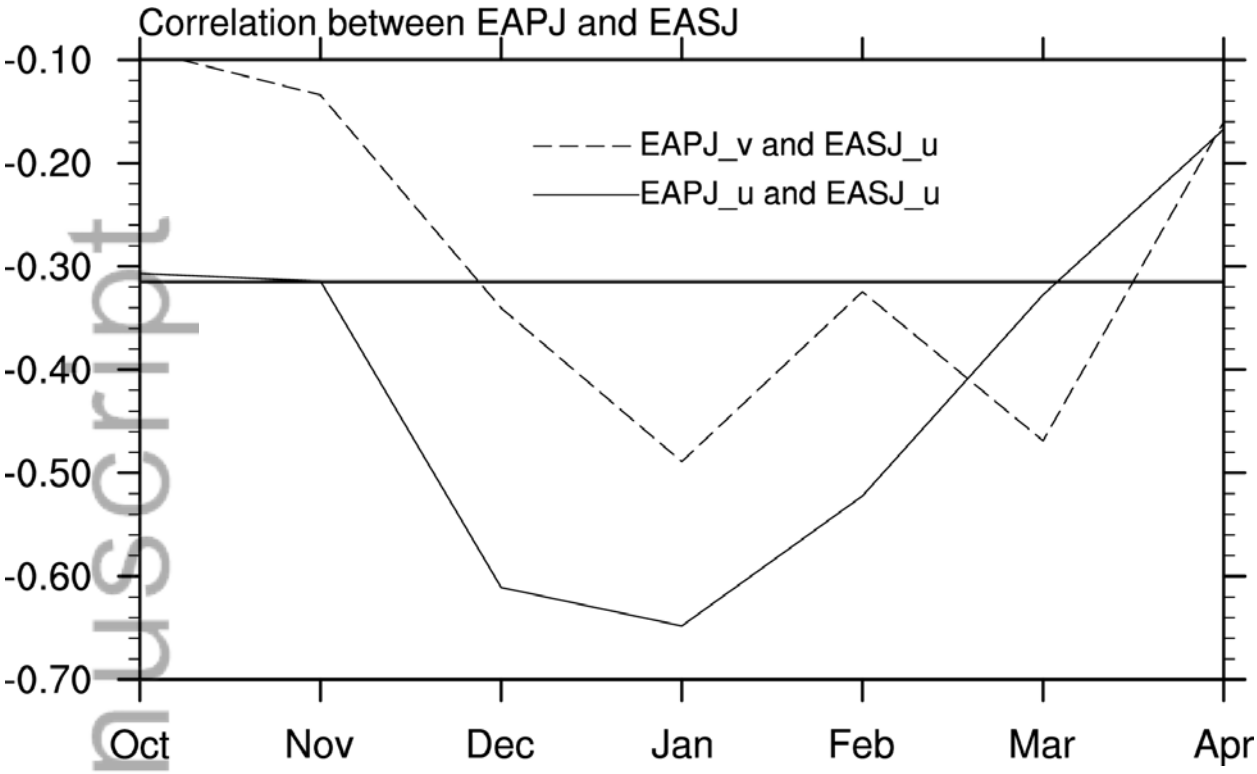

Figure 7. The subseasonal variation of the correlation coefficient between the zonal wind in EASJ (EASJ_u) and the zonal wind in EAPJ (EAPJ_u, solid line), and the meridional wind in EAPJ (EAPJ_v, dash line). The horizontal line denotes the level of 95% confidence.

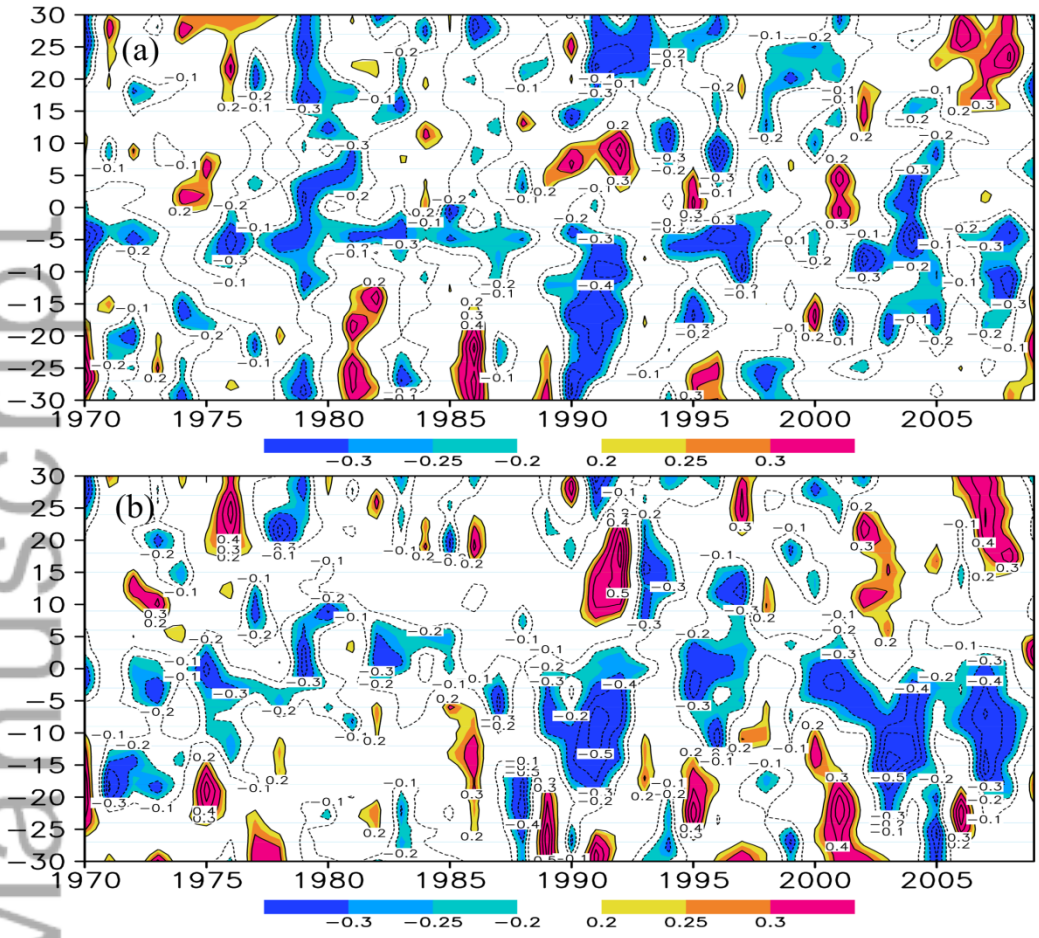

Figure 8. (a) The interannual variation of the lead-lag correlation between the area-mean zonal wind in EAPJ and EASJ-O. The Y coordinate is the days when EAPJ lags EASJ-O. (b) same as (a), but for the relation between the area-mean zonal wind in EAPJ and EASJ-L.

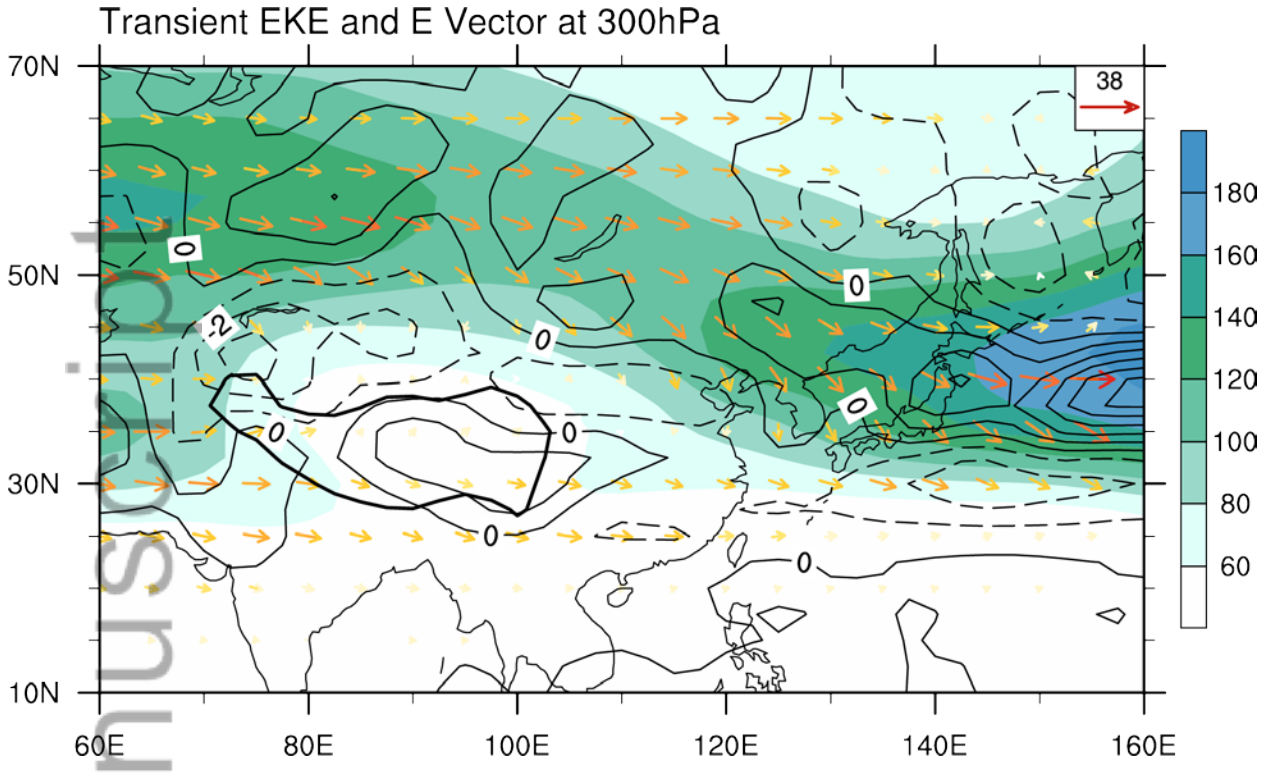

Figure 9. Climatological distributions of transient EKE (shading, $m^2\ s^{-2}$), vector ***E*** ($m^2\ s^{-2}$), and the divergence of ***E*** (contour, $10^{-5}\ m\ s^{-2}$) at 300 hPa.

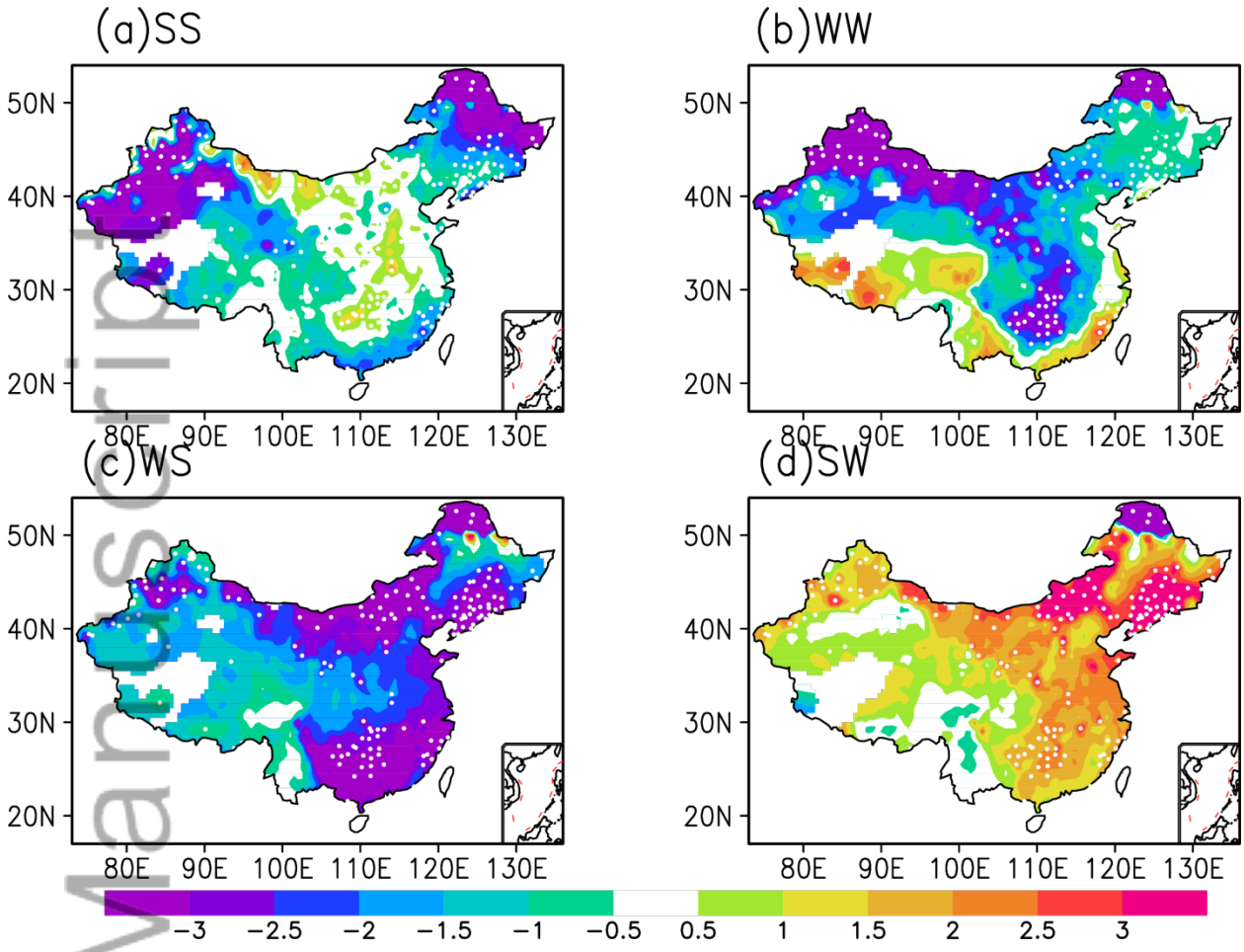

Figure 10. Composite surface temperature anomalies (°C) in China for different matchups of EASJ and EAPJ (listed in Table 2). The open circle denotes the station statistical significant at 95% confidence level with Student's *t*-test.

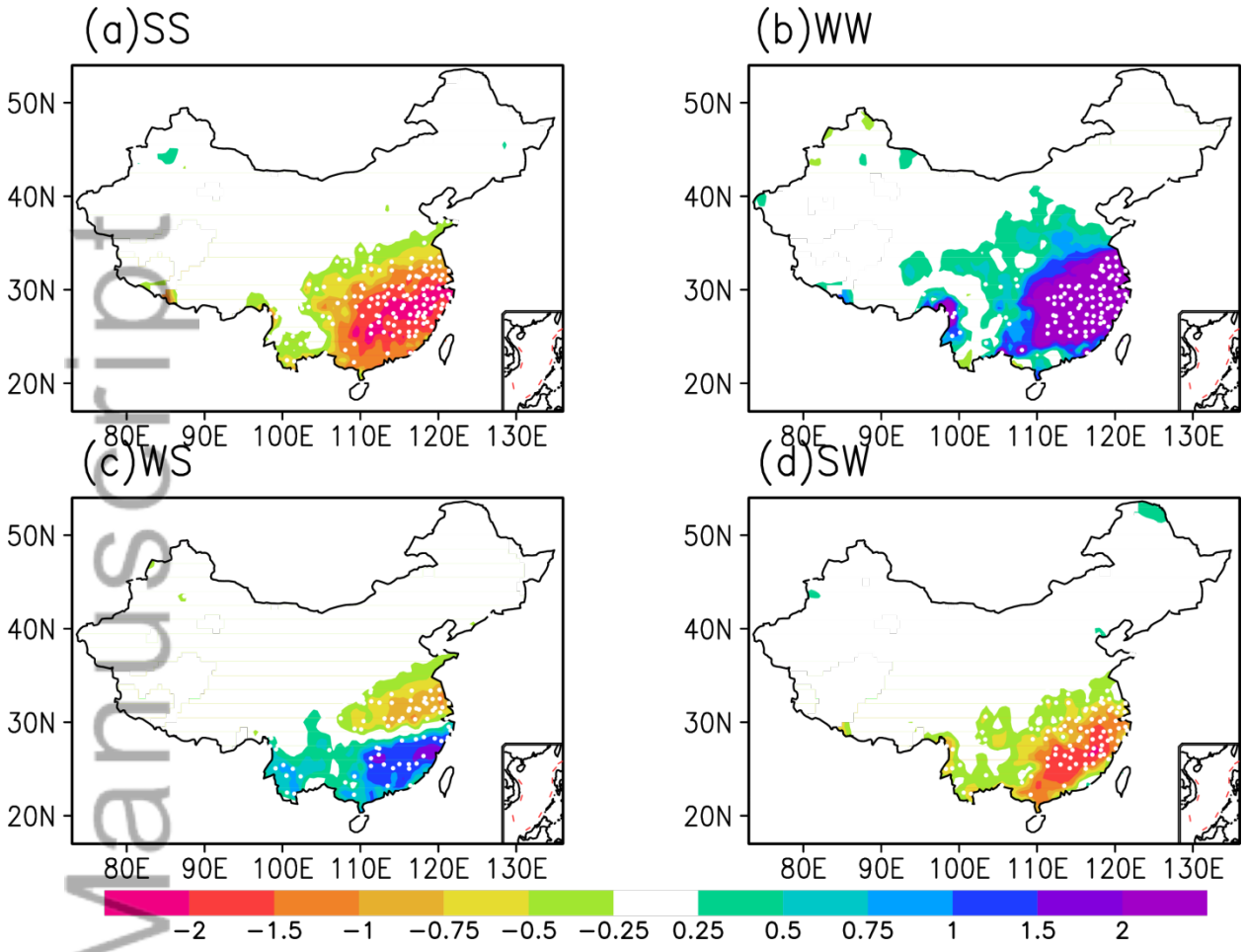

Figure 11. Same as Figure 10, but for the precipitation anomalies (mm/day).

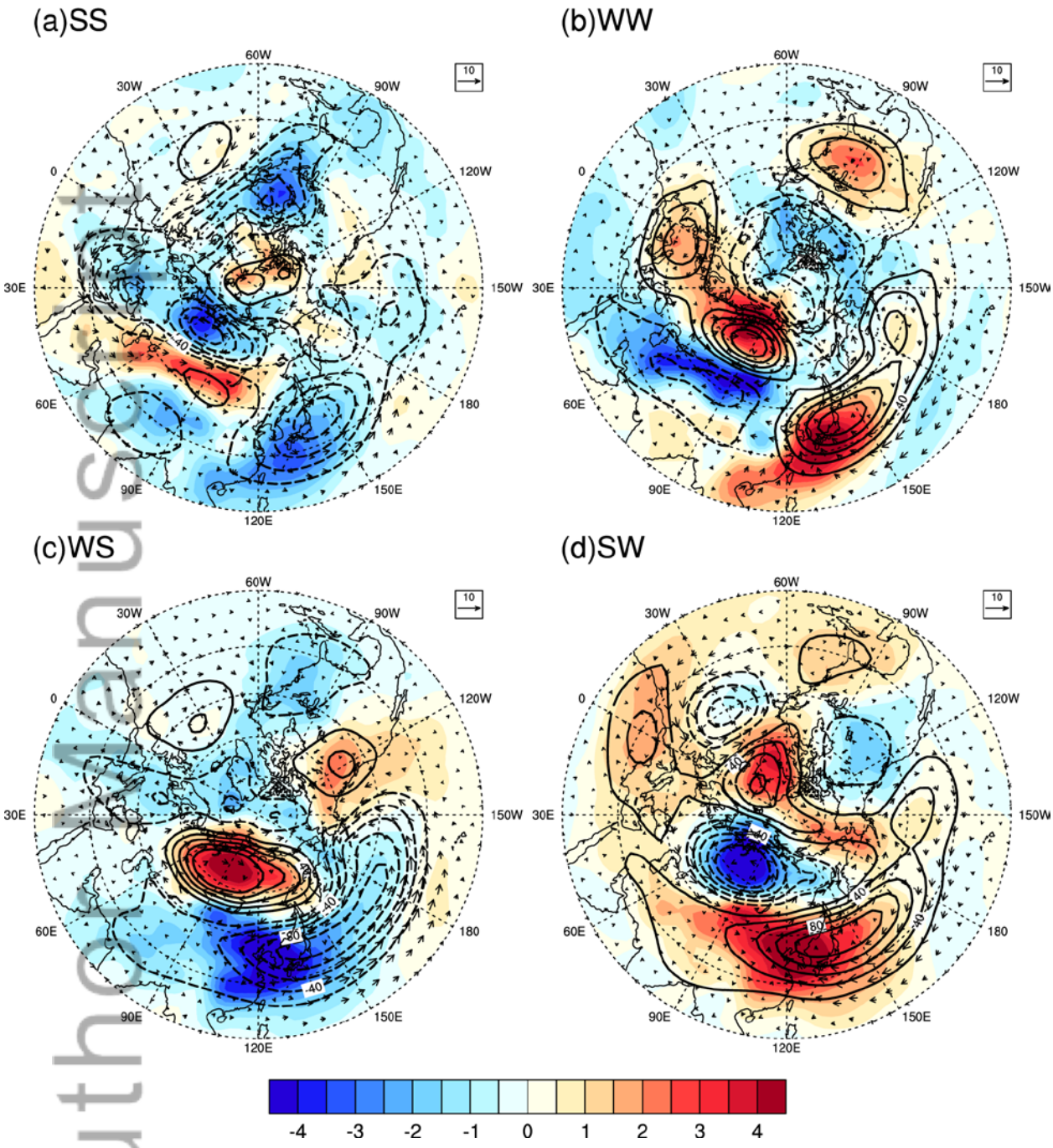

Figure 12. (a) Composite circulation anomalies for SS (SS pentads mean minus the climatology). The geopotential height (gpm) at 500 hPa is denoted by contours, air temperature (°C) at 850 hPa

by shaded areas, and wind at 850 hPa by vectors (m s^{-1}). (b) , (c), and (d) for WW, WS, and SW, respectively.